



# Numerical Investigation of an Innovative Windbreak Design with Jet Flow Generated by an Air Curtain for Half-pipe Skiing

K. Liu<sup>1, 2, 3</sup>, F. Liu<sup>2</sup> and Q. Liu<sup>1, 2, 3, †</sup>

<sup>1</sup> State Key Laboratory of Mechanical Behavior and System Safety of Traffic Engineering Structures, Shijiazhuang, Hebei, 050043, China

<sup>2</sup> School of Civil Engineering, Shijiazhuang Tiedao University, China

<sup>3</sup> Innovation Center for Wind Engineering and Wind Energy Technology of Hebei Province, China

†Corresponding Author Email: [lqk@stdu.edu.cn](mailto:lqk@stdu.edu.cn)

## ABSTRACT

The sport of half-pipe skiing, characterized by its dynamic maneuvers and high-speed descents, often faces challenges posed by unpredictable wind conditions. To address this, an advanced wind-blocking system incorporating an air curtain capable of generating a jet flow is proposed. This pioneering design offers a dual advantage: the system can significantly reduce the windbreak size in the vertical dimension while maintaining a satisfactory wind-blocking effect. A comprehensive study is conducted to analyze the effects of the height of the windbreak and the jet emission angle from the air curtain. When the jet speed is 40 m/s, a 50° emission angle and a 2 m height of the windbreak result in an optimal wind-blocking effect. Furthermore, delving deeper to understand the underpinnings of this phenomenon, we discovered that a counterrotating vortex pair, which forms in the presence of this jet under crossflow conditions, plays a pivotal role in augmenting the wind-blocking capabilities of the system.

## Article History

Received October 25, 2023

Revised December 12, 2023

Accepted January 5, 2024

Available online March 27, 2024

## Keywords:

Windbreak

Air curtain

Wind-blocking effect

Jet in a crossflow

Numerical simulation

## 1. INTRODUCTION

Wind can have significant effects on certain winter sports, particularly those that involve jumping or flying, such as half-pipe skiing. Some of these effects can cause negative consequences, not only on the performance of athletes in competition but also on their physical health (Hamlet, 1988; Suresh, 2006; Nanda, 2012). In the recent Winter Olympics, high winds caused disruptions, resulting in multiple injuries (TRTWorld, 2023; Bushnell, 2023; Mullin, 2023). To minimize the impact of crosswind on athletic performance and reduce the risk of physical injury, windbreaks have been developed and implemented in the fields of several winter sports, including half-pipe skiing and freestyle skiing aeriels. Additionally, the International Ski Federation (FIS) established a standard for the windbreak utilized in these winter sports. This standard focuses primarily on the wind-blocking effect and the appearance of the windbreak to simultaneously provide both a low-wind sports field and an optimal viewing experience.

Currently, traditional wall-like windbreaks are primarily implemented for winter sports. This type of windbreak, located outdoors (Li et al., 2007; Zhang et al., 2017; Fang et al., 2018) or inside buildings (Heisler, 1991;

Zhu et al, 2022; Cameron et al, 2015), has been studied for decades. Our group designed and provided construction guidance for the windbreak system utilized in the half-pipe skiing and freestyle skiing aeriels events in the 2022 Beijing Winter Olympics. During this process, the traditional windbreak was realized to have several drawbacks. First, the height needs to reach 14-15 m to satisfy the wind-blocking requirement of the standard set by the FIS. The structural robustness of such a tall windbreak under high wind speed conditions should be rigorously evaluated. Thus, the material of the windbreak must be sufficiently strong, which adds more difficulty to the production and installation and even more cost to the windbreak. Second, traditional windbreaks are opaque. As winter sports are both participatory and spectator events, they require global broadcasting and streaming to reach audiences worldwide, particularly in major events such as the Winter Olympics. Therefore, designing traditional windbreaks for winter sports requires considering not only the wind-blocking effect but also the viewing experience. In addition, the viewing experience of winter sports includes the aesthetics of the windbreaks themselves, which means that the design of these tall structures must be visually appealing. This presents an additional challenge for the design of windbreaks. Therefore, based on the two aforementioned points and the concept of the

Nomenclature			
$h$	windbreak height	$Z_c$	height of the marked region
$U_\infty$	freestream velocity magnitude	$z$	distance in the vertical direction
$V$	jet velocity magnitude	$\lambda$	wind environment coefficient
$\beta$	ratio between the jet velocity and the freestream velocity	$u$	wind speed
$\alpha$	jet emission angle	$U_e$	equivalent wind speed
$\delta$	distance in the spanwise direction	$\eta$	wind-blocking efficiency

“High-tech Winter Olympics”, developing windbreaks utilized in winter sports, such as half-pipe skiing, to reduce their size and make them more technologically advanced is crucial.

Researchers (Park & Lee, 2003; Dong et al., 2007; Chu et al., 2013; Li & Sherman, 2015; Gillies et al., 2017; Jiang et al., 2019; Tominaga & Shirzadi, 2022) have used fence-like windbreaks to protect highways, railways and airports from wind, sand, snow and dust. This type of windbreak was successfully implemented in the National Alpine Skiing Center in the 2022 Beijing Winter Olympics (Fu & Li, 2023). However, this type of porous and translucent windbreak cannot completely solve the issues mentioned above because the size of the structure is still relatively large. To address this, this study creatively introduces an air curtain that can generate jet flow for the windbreak system to reduce the vertical dimension and maintain an adequate wind-blocking effect.

Notably, this air curtain will lead to an unsteady flow condition named the jet in a crossflow (JICF), which refers to the semibounded flow in which a flux of fluid at a lower bounding wall interacts with the main flow above. The behavior of the JICF is mainly determined by the velocity ratio between the jet flow and the freestream (Margason, 1993; New et al., 2006). To study the interaction between the jet flow and the freestream, some researchers (Sau & Mahesh, 2008; Bidan & Nikitopoulos, 2013; Cambonie & Aider, 2014; Klotz et al., 2019) have investigated this situation in the low velocity ratio regime and observed hairpin instability. Meanwhile, other studies (Mahesh, 2013; Klotz et al., 2014; Regan and Mahesh, 2017; Gevorkyan et al., 2018) have focused on the JICF phenomenon with large velocity ratios. Moreover, under large velocity ratios, researchers also used a fluid-structure interaction approach to investigate the influence of the JICF on airfoils or vehicles at low Reynolds numbers (Jones and Yamaleev, 2012; Perrotta & Jones, 2017; Poudel et al., 2021). Herein, the velocity ratio between the jet flow produced by the air curtain and the freestream is relatively large, 4.0, based on the field test of the 2022 Beijing Winter Olympics.

### 1.1 Contributions

The current study presents an innovative design of a windbreak system with an air curtain. Both two-dimensional (2D) and three-dimensional (3D) numerical simulations are conducted and compared. The results show that the 3D effect in this system is almost negligible. The results also demonstrate that this design can reduce the height of the windbreak from 14-15 m to 2 m while maintaining a satisfactory wind-blocking effect. Meanwhile, a counterrotating vortex pair (CRVP) is

observed in the simulations, which is consistent with the previous experimental and numerical studies. Additionally, the wind-blocking effect achieved by this system can be explained by the CRVP.

### 1.2 Paper overview

In Section 2, the numerical methods and simulation setup are introduced. Verification and validation of the computational model, including the comparison between the 2D and 3D models, are also presented in this section. In Section 3, numerical results are presented and discussed. Specifically, in Section 3.1, the effect of the height of the windbreak in this system is analyzed in combination with the jet flow generated by the air curtain. In Section 3.2, the optimal jet emission angle is investigated. In Section 3.3, the CRVP phenomenon in these simulations is described and analyzed. Section 4 concludes the study and discusses possible future works.

### 1.3 Nomenclature

List of symbols

## 2. METHODOLOGY

### 2.1 Computational Model of the Half-Pipe Skiing Venue

In this study, both two-dimensional (2D) and three-dimensional (3D) models of the half-pipe skiing venue are implemented. The results of the 2D and 3D models are compared to determine the existence of a 3D effect in the simulations. The 2D schematic diagram of the region near the half-pipe skiing venue is shown in Fig. 1. As shown in Fig. 1(a), there exists a windbreak with a thickness and a flexible height  $h$  in the upstream region. The nozzle of the air curtain is located in the middle part at the top of the windbreak, which can emit a jet flow at varying speeds  $V$  and angles  $\alpha$ . Note that  $\alpha$  is the angle between the jet emission direction and the horizontal direction ( $x$  direction). The half-pipe venue is in the downstream region. Note that its shape and size, which are also presented in Fig. 1(a), are determined by the real object at the 2022 Beijing Winter Olympics. Figure 1(b) shows that the computational domain has a width of 1200 meters, which is approximately 200 times the depth of the half-pipe skiing venue, and a height of 400 meters. The boundary conditions are also illustrated in Fig. 1(b). The maximum freestream velocity is 10 m/s and is unidirectional, which is based on the field test in the 2022 Beijing Winter Olympics.

The 3D model is shown in Fig. 2. These 3D models are adopted by extruding the 2D model  $\delta=6$  m and 0.6 m in the spanwise direction. By enforcing periodic boundary

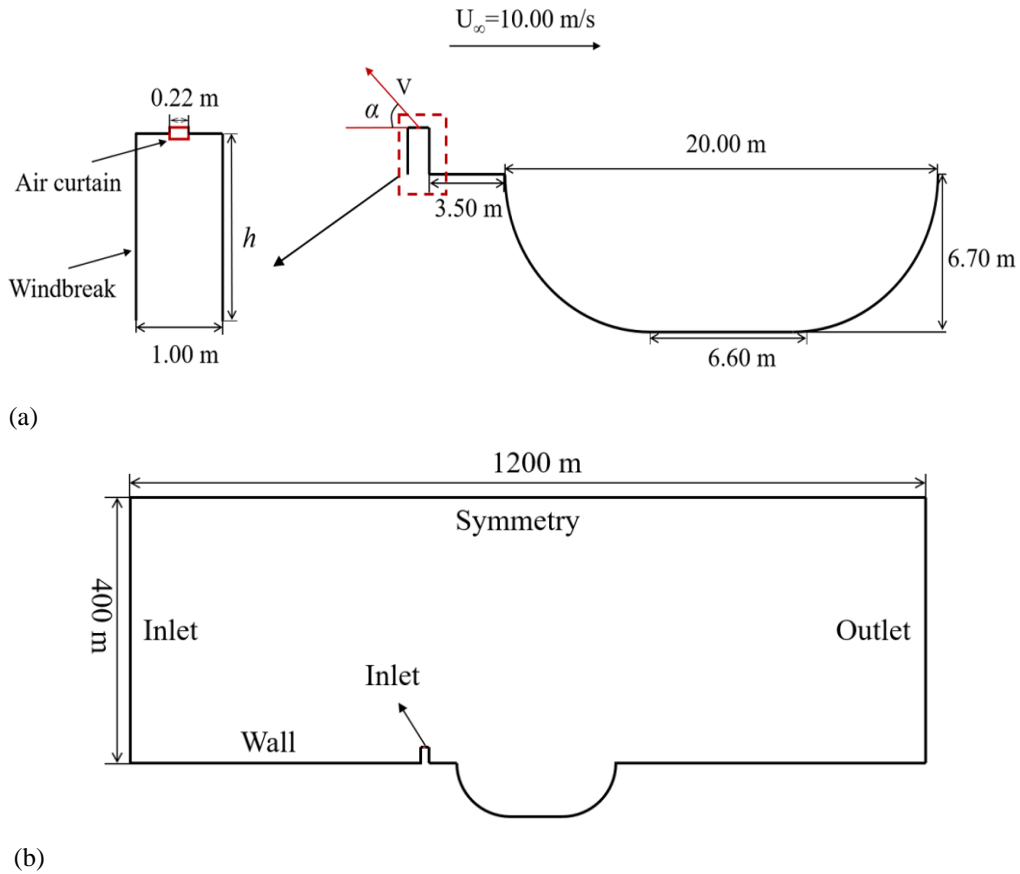


**Fig. 1** Schematic diagram of (a) the region near the half-pipe skiing venue and (b) the whole computational domain of the 2D model

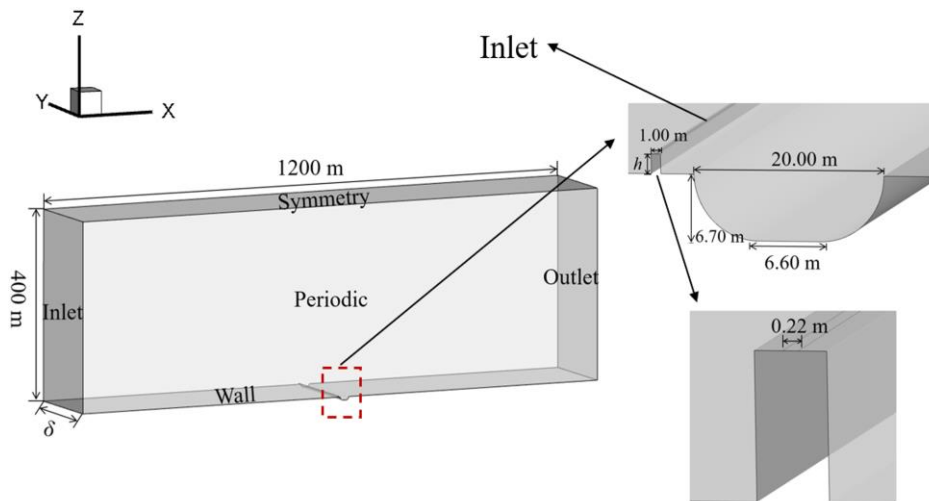


**Fig. 2** Schematic diagram and boundary conditions of the 3D model

conditions on both spanwise surfaces, a half-pipe skiing venue with an infinite length is generated.

A numerical simulation is conducted under an inlet freestream velocity of 10 m/s, which is based on the field test during the 2022 Beijing Winter Olympics. The ratio between the jet velocity and this freestream velocity is introduced, which is given by  $\beta$ . To minimize the impact

of wind on the athlete, the FIS standardizes that in the area (0.5 m to 26.5 m in the  $x$  direction and -6.7 m to 8 m in the  $y$  direction) shown in Fig. 3, the wind velocity magnitude needs to be restricted to below 3.5 m/s. To provide better observation space and wind-blocking efficiency for this sport, the optimal design of this system should achieve the wind speed standard, which should be lower than 3.5 m/s,

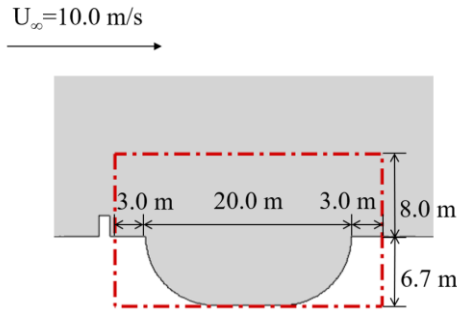


**Fig. 3 Critical area where the wind speed needs to be restricted**

with a lower height of the windbreak and an optimal jet emission angle of the air curtain.

Note that after obtaining the wind velocity magnitude in the marked region, a parameter named the wind environment coefficient  $\lambda$  is quantified to measure the wind-blocking efficiency  $\eta$  of this system. The wind environment coefficient is defined as follows:

$$\lambda = \frac{U_e}{U_\infty} \quad (1)$$

Herein,  $U_e$  is the equivalent wind speed, and it can be defined as:

$$U_e^2 = \frac{1}{Z_c} \int_0^{Z_c} u^2(z) dz \quad (2)$$

where  $Z_c$  is the height of the marked region where the wind speed needs to be restricted, which is 8 m in this simulation, as shown in Figure 4, while  $z$  is the distance in the vertical direction.  $u$  is the wind speed, which can be complex and fluctuating, along two segments A and B in the vertical direction, as presented in Fig. 4. Notably, A in the upstream region and B in the downstream region are located at the edges of the half-pipe skiing venue, which are the essential zones for athletes affected by wind disturbance during competition.

After the equivalent wind speed  $U_e$  is calculated, the wind-blocking efficiency can be specified as:

$$\eta = 1 - \lambda \quad (3)$$

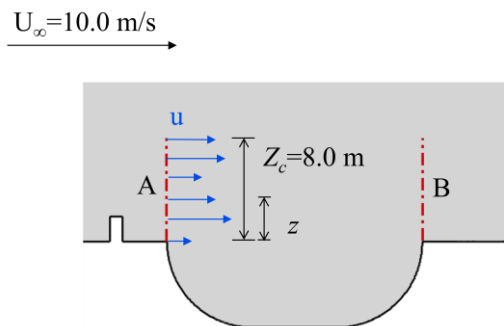


**Fig. 4 Schematic diagram of the measurement setup for the wind-blocking efficiency**

**Table 1 Summarization of simulation parameters**

Input Variable	Value/Setting
Turbulence model	SST k- $\omega$
Pressure-velocity coupling	SIMPLEC
Spatial discretization scheme	Second-order upwind
Time integration	Second-order implicit
Inlet turbulence viscosity ratio	0.2
Convergence criterion for residuals	$10^{-4}$
Inner iterations	30
Reynolds number	$4.8 \times 10^6$

The unsteady Reynolds-averaged Navier–Stokes (URANS) SST k- $\omega$  turbulence model is used in all flow simulations presented in this study. For pressure-velocity coupling, the Semi-Implicit Method for Pressure Linked Equations-Consistent (SIMPLEC) algorithm with a second-order upwind spatial discretization scheme is utilized to solve the RANS equations. A second-order implicit transient formulation is selected to ensure the time integration accuracy. The inlet turbulence viscosity ratio of both the freestream and jet is set to 0.2 to obtain a relatively uniform estimation of the turbulence. Additionally, for each inner iteration, the residual convergence criterion is fixed at  $10^{-4}$  for better converged results. The number of inner iterations is set to 30. For all the simulations, the Reynolds number based on the depth of the half-pipe skiing venue and the freestream velocity is approximately  $4.8 \times 10^6$ . The numerical setup is summarized in Table 1.

## 2.2 Verification and Validation

Quadrilateral and hexahedral meshes are generated using the commercial meshing software ANSYS® ICEM® for the 2D and 3D numerical simulations. Since second-order accurate numerical methods are used in all simulations, fine meshes are required near the wall boundary to capture the potential intricate vortex dynamics. Meshes of the 2D and 3D models are shown in Fig. 5 (a) and (b). To ensure that the numerical results are independent of the mesh resolution, a mesh refinement study is carried out using four sets of 2D meshes. Therein, the coarse mesh consists of 30551 elements, the medium mesh consists of 127161 elements, the fine mesh consists of 460416 elements and the finer mesh consists of 805488 elements. The refinement is simultaneously carried out in both the horizontal and vertical directions. The mesh refinement study is conducted for a windbreak with a height of 2.0 m, freestream velocity  $U_\infty = 10$  m/s, air curtain velocity  $V = 40$  m/s (which leads to  $\beta = 4.0$ ) and jet emission angle  $\alpha = 30^\circ$ . The velocity magnitude at three points (P1, P2 and P3) located in the critical area (shown in Fig. 6 (a)) is investigated to evaluate the mesh quality. The results of the mesh refinement study are presented in Table 2. Table 2 shows that there is a minuscule discrepancy between the medium mesh, the fine mesh and the finer mesh, even at P1, which is located in the interaction area between the freestream flow and the jet flow. Therefore, considering the computational cost, the medium mesh is selected to conduct all the simulations.

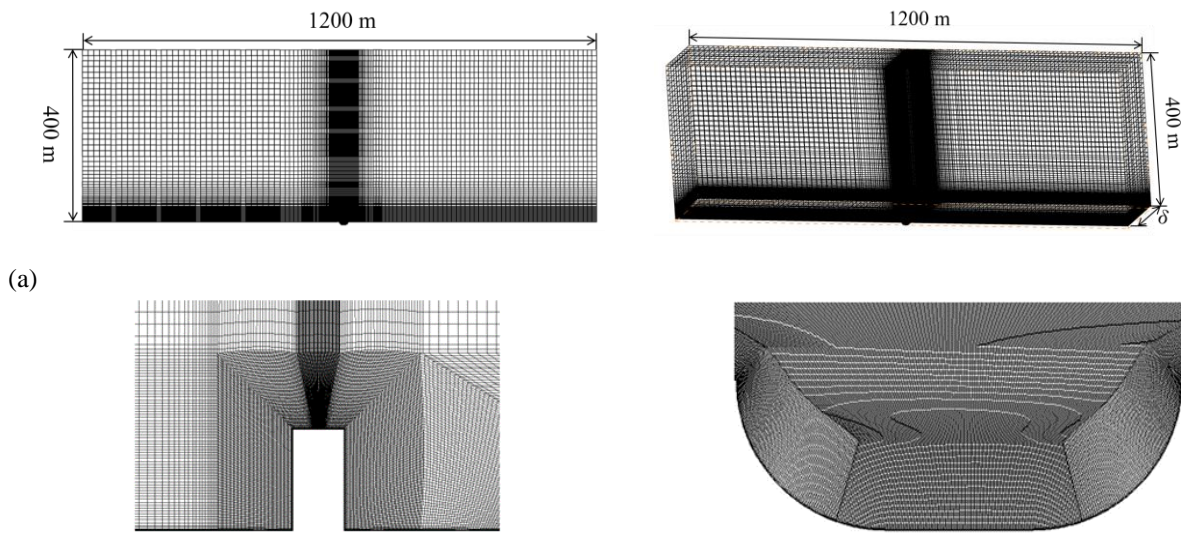


Fig. 5 (a) Meshes of the 2D and 3D models; (b) mesh near the air jet and in the Half-Pipe region

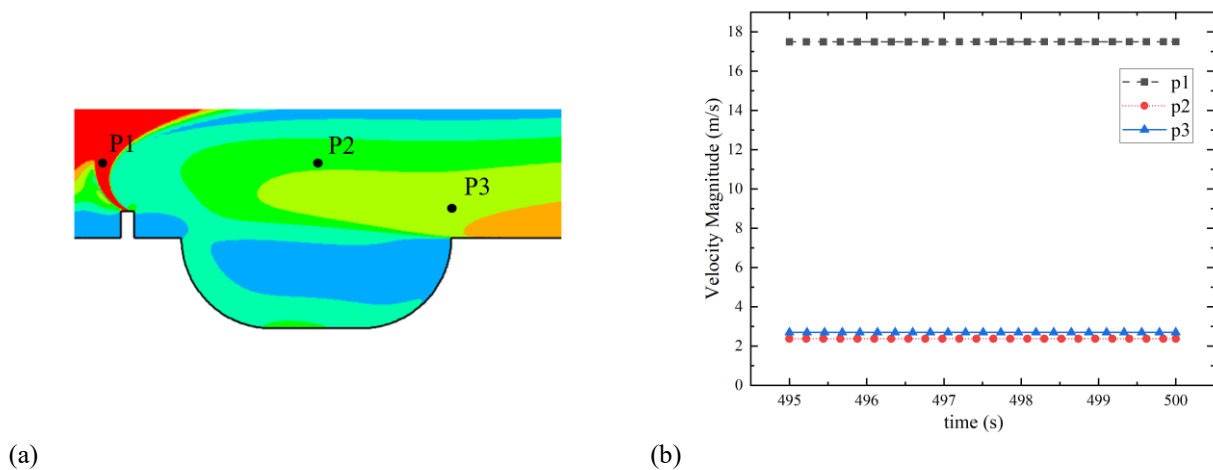


Fig. 6 (a) Observation points for numerical verification; (b) instantaneous velocity magnitude history of the observation points

Table 2 Results from the mesh refinement study

Number of elements	P1		P2		P3	
	Velocity magnitude (m/s)	Percent difference	Velocity magnitude (m/s)	Percent difference	Velocity magnitude (m/s)	Percent difference
30551	15.73	-	2.30	-	2.68	-
127161	17.77	12.97%	2.37	3.04%	2.69	0.37%
460416	16.90	4.90%	2.46	3.80%	2.80	4.09%
805488	17.28	2.25%	2.38	3.25%	2.71	3.21%

Additionally, the mean nondimensional wall distance  $y^+$  for all wall boundaries in the simulations, including the 2D and 3D models with different turbulence models, is less than 1.

To investigate the effect of the time step size, simulation results obtained using various time steps (0.01 s, 0.004 s, 0.001 s and 0.0005 s) are compared. The same observation points (P1, P2 and P3) as mentioned above are utilized for this investigation. This time step comparison is presented in Table 3, from which the difference between

the results for 0.004 s, 0.001 s and 0.0005 s can be observed to be trivial. Thus, to save computational cost, the time step  $dt = 0.004$  s is selected for all the simulations presented in the remainder of the paper. Furthermore, note that all data presented in this study are collected after a stable wind speed stage is reached in the critical area of all simulations, which occurs after 450 seconds. Figure 6 (b) presents the instantaneous velocity magnitude of the three observation points during 495 s to 500 s. It can be seen that the fluctuations are negligible.

**Table 3 Results from the time step size study**

Time step size (s)	P1		P2		P3	
	Velocity magnitude (m/s)	Percent difference	Velocity magnitude (m/s)	Percent difference	Velocity magnitude (m/s)	Percent difference
0.01	15.76	-	2.38	-	2.72	-
0.004	17.77	12.75%	2.37	0.42%	2.69	1.10%
0.001	17.98	1.18%	2.36	0.42%	2.70	0.37%
0.0005	18.38	2.22%	2.37	0.42%	2.68	0.74%

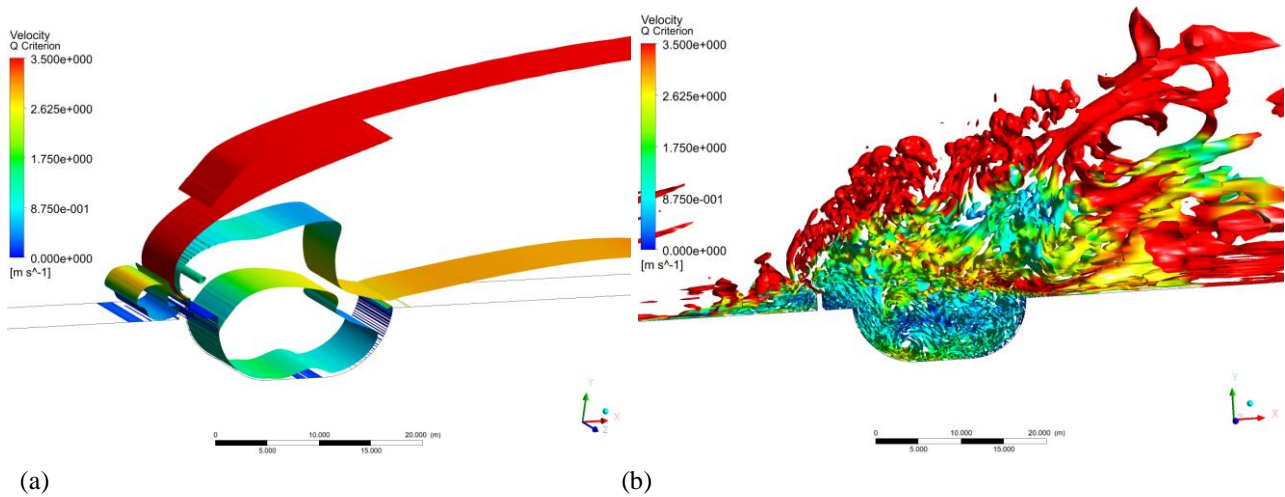


**Fig. 7 Structures in the spanwise direction represented by the isosurface of the Q criterion with a value of  $5.2 \times 10^{-4}$  from the (a) SST  $k-\omega$  model and (b) LES model**

Three 3D models are established to evaluate the impact of the 3D effect: SST  $k-\omega$  ( $\delta=6$  m and  $\delta=0.6$  m) and large-eddy simulation (LES). Note that all the other setup conditions of the 3D simulation are exactly the same as in the 2D simulation. Figure 7 shows the vortex structures in the spanwise direction represented by the isosurface of the Q criterion with a value of  $5.2 \times 10^{-4}$  from the two 3D models. These isosurfaces are colored by the velocity magnitude. For the LES model, the separated vortex structure is more pronounced, which agrees well with previous research (Liu et al., 2019). However, note that this study primarily concentrates on the velocity magnitude. Therefore, to demonstrate the deviation between different models, the mean velocity magnitude in the spanwise direction for these 3D models and that obtained with the 2D SST  $k-\omega$  model are compared in Fig. 8. These magnitudes are measured along a segment in the streamwise direction ( $x$  is from 0.5 m to 26.5 m, which covers the critical region of the half-pipe venue) at a height of  $z = 2.0$  m. Figure 8 shows that first, the trajectories of the 2D and 3D SST  $k-\omega$  models largely coincide, indicating similar velocity magnitudes in these cases. Additionally, the trajectory from the 3D LES model closely aligns with that obtained by the 2D model. Particularly in the region where  $x$  ranges from 0.5 m to 20.0 m, the mean velocity magnitude of the 3D LES model exhibits only a minor variation compared to that generated by the 2D SST  $k-\omega$  model. Even in the adjoining region ( $x$  ranges from 20.0 m to 26.5 m), the deviation is less than 20%. Generally, the results from the 3D LES model agree reasonably with those from the 2D model, which means that the turbulence effect on the instantaneous velocity profile in this problem is not significant. Therefore, all the

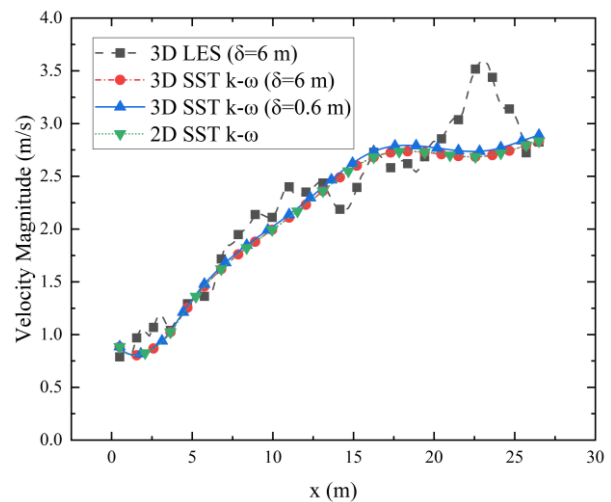


**Fig. 8 Mean velocity magnitude obtained by different models from  $x=0.5$  m to  $x=26.5$  m at a height of  $z = 2.0$  m**

simulations in the remainder of the paper are conducted with the 2D model to save computational cost.

### 3. RESULTS AND DISCUSSION

#### 3.1 Effect of Various Windbreak Heights on the System

Normally, the height of the traditional windbreak for half-pipe skiing sports is 14 m to 15 m. Therefore, reducing the height of the windbreak could enhance the

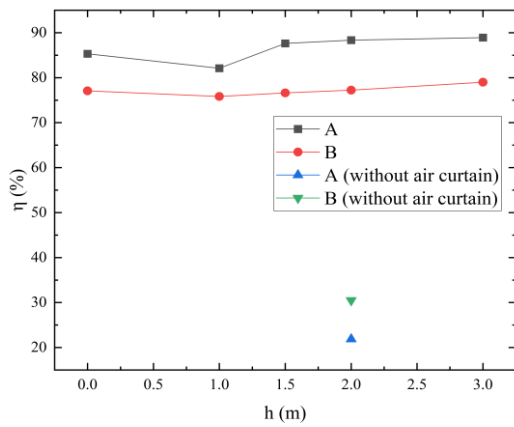


**Fig. 9** Wind-blocking efficiency for different windbreak heights when  $V$  is 40 m/s ( $\beta$  is 4.0) and  $\alpha$  is  $30^\circ$

feasibility of producing and installing the windbreak system while also improving the observational capabilities in the half-pipe skiing competition.

The first step of this study is to estimate the wind-blocking efficiency for various windbreak heights under the conditions that the jet flow speed  $V$  is 40 m/s ( $\beta$  is 4.0) and the emission angle  $\alpha$  is  $30^\circ$ . The wind-blocking efficiency tested at vertical lines A upstream and B downstream (shown in Fig. 4) with various windbreak heights is presented in Fig. 9. Note that a case without an air curtain jet is also included. Generally, Fig. 9 shows that without the air curtain jet, the wind-blocking efficiency is low, approximately 30%, even when there exists a 2 m height windbreak. While the air curtain is working, the wind-blocking efficiency is significantly higher than that without the air curtain. The wind-blocking efficiency  $\eta$  can reach over 75% on both segments A and B. Particularly, when there is a jet flow, the  $\eta$  on segment A can achieve nearly 90% with a 3 m windbreak. From the trajectories, the  $\eta$  on segment A can be observed to be constantly higher than that on B because the distance between the air curtain nozzle and segment A is shorter. Moreover, the value of  $\eta$  slightly ascends on segment A when the windbreak height increases from 0 m to 1.5 m.

After the height reaches 1.5 m, the trajectories become smoother as the height of the windbreak increases. For the wind-blocking efficiency on segment B, the value gradually rises as the windbreak height increases.

Second, to deeply investigate the wind-blocking effect, the velocity distribution is displayed in Fig. 10, where the maximum velocity magnitude in the color legend is set to 3.5 m/s. Thus, the regions with higher velocity magnitudes are obviously marked. As shown by Fig. 10(a) to (c), although the air curtain provides a fairly good wind-blocking efficiency, there still exist regions where the wind speed exceeds 3.5 m/s or is relatively large inside the critical area when the windbreak height is less than 2 m. Specifically, these regions are near the right edge of the half-pipe skiing venue and the upper left corner of the critical area. As the windbreak height increases, the wind velocity magnitude in these regions inside the critical area is mitigated. Eventually, after the height of the windbreak reaches 3 m, these regions disappear, indicating that the wind velocity magnitude within them satisfies the 3.5 m/s standard. Although compared to the traditional 15 m height windbreak currently utilized in the half-pipe skiing, the 3 m windbreak is significantly small, the observation space and angle in this study still must be improved, which requires a lower height of the windbreak. Thus, in this study, the height of the windbreak is set to 2 m.

To demonstrate the suitability of the air curtain system with a 2 m windbreak, velocity magnitudes along several horizontal segments, which are shown in Fig. 11(a), are measured. Note that these segments are evenly vertically distributed within the critical area with a 2 m interval. Figure 11(b) shows the result without the air curtain, in which almost all the wind velocity magnitudes in the region above the windbreak can be clearly detected to exceed the limit. This phenomenon is consistent with the observation of the velocity distribution presented in Fig. 10(f). However, with the implementation of the air curtain, the wind velocity magnitudes sharply decrease in these regions, as shown in Fig. 11(c). Only in a relatively tiny region near the upper left corner does the wind velocity magnitude exceed the limit velocity of 3.5 m/s.

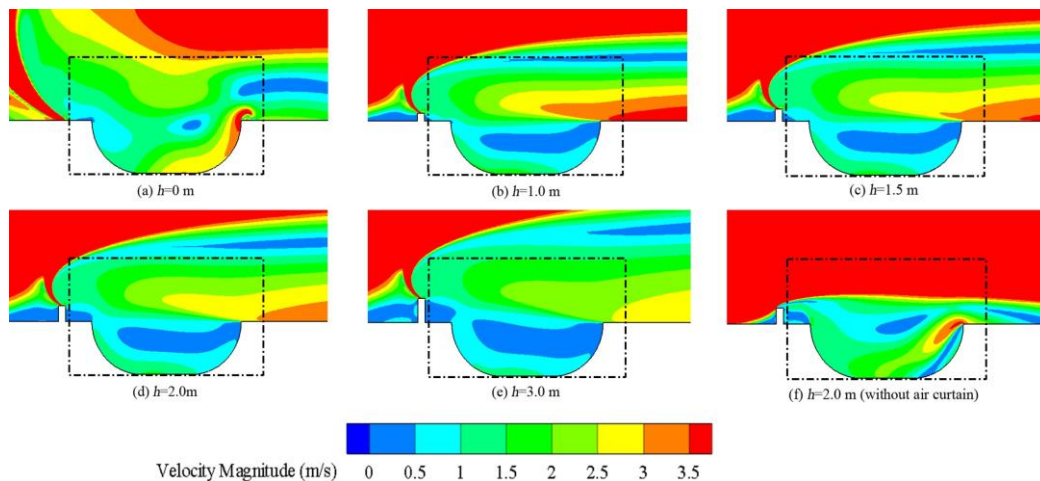
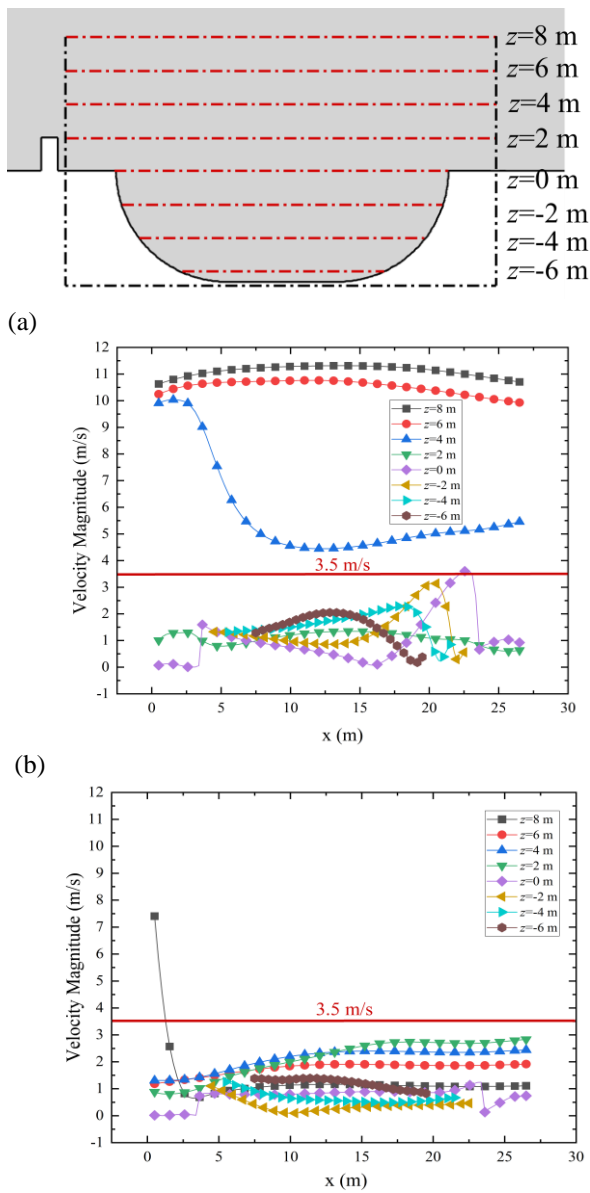


**Fig. 10** Velocity magnitude field at various windbreak heights when  $V$  is 40 m/s ( $\beta$  is 4.0) and  $\alpha$  is  $30^\circ$



(a) Horizontal segments for collecting the data of the wind velocity magnitude; (b) wind velocity magnitude with only the 2 m height windbreak; (c) wind velocity magnitude with the 2 m height windbreak and air curtain

Figure 10(d) shows that this region occupies only a small area, which is negligible. Therefore, this air curtain system with a 2 m windbreak satisfies the standard set by the FIS.

### 3.2 Effect of the Jet Emission Angle of the Air Curtain on the System

After the height of the windbreak is fixed to 2 m, the optimal jet emission angle  $\alpha$  of the air curtain, which is shown in Fig. 1(a), must be found. Multiple angles from  $20^\circ$  to  $70^\circ$  are tested in the simulations. The wind-blocking efficiency  $\eta$  values on segments A and B (shown in Fig. 4) for different angles are presented in Fig. 12. The wind-blocking efficiency  $\eta$  on both segments A and B has relatively high values with different jet emission angles. These values are significantly larger than those without the air curtain, as shown in Fig. 9. Meanwhile, the wind-blocking efficiency  $\eta$  is consistently higher on segment A,

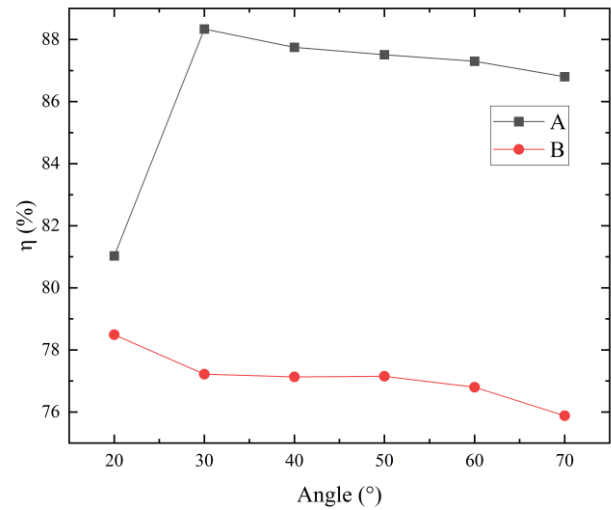


**Fig. 12** Wind-blocking efficiency for different jet emission angles when  $V$  is 40 m/s ( $\beta$  is 4.0) and  $h$  is 2 m

which is closer to the wind curtain, than that on segment B. This observation is in good agreement with the findings shown in Fig. 9. Additionally, the wind-blocking efficiency on segment A reaches the maximum value (over 88%) when the angle  $\alpha$  is  $30^\circ$  and then gradually decreases with a larger emission angle. In contrast, the  $\eta$  on segment B has a continuous slight decrease from  $\alpha=20^\circ$  to  $\alpha=70^\circ$ . Note that the minimum value of  $\eta$  on segment A is approximately 81%, while that on segment B is over 75%. The velocity magnitude distributions are displayed in Fig. 13. The maximum wind-blocking efficiency on segment A occurs when the jet emission angle  $\alpha$  is  $30^\circ$ ; nevertheless, there still exist regions at the upper left corner of the critical area shown in Fig. 13(b) where the wind velocity magnitude exceeds the limit.

However, when the jet emission angle rises from  $40^\circ$  to  $60^\circ$ , these high-speed regions are eliminated. Comparing the velocity distribution fields obtained at angles of  $\alpha=40^\circ$  (Fig. 13(c)) and  $\alpha=60^\circ$  (Fig. 13(e)) to the field obtained when  $\alpha=50^\circ$  (Fig. 13(d)), the distance between the high-speed region on the right side of the half-pipe venue and its right edge can be observed to be the largest when  $\alpha=50^\circ$ .

Similar to in Section 3.1, when the jet emission  $\alpha$  is  $50^\circ$ , the velocity magnitudes at multiple horizontal segments in the critical area are presented in Fig. 14. This figure indicates that the velocity magnitudes in the whole critical area are below 3.5 m/s, which differs from those at an  $\alpha$  of  $30^\circ$ , as shown in Fig. 11(c), and satisfies the standard set by the FIS.

Conclusively, the jet emission angle of  $50^\circ$  leads to the farthest distance between the high-speed region on the right side and the edge of the half-pipe venue. This distance is sufficient to minimize the effect of the high-speed region on the critical area. Additionally, the velocity magnitude in the whole critical area still meets the FIS standard. Therefore, based on these considerations, the optimal jet emission angle is set to  $50^\circ$ .

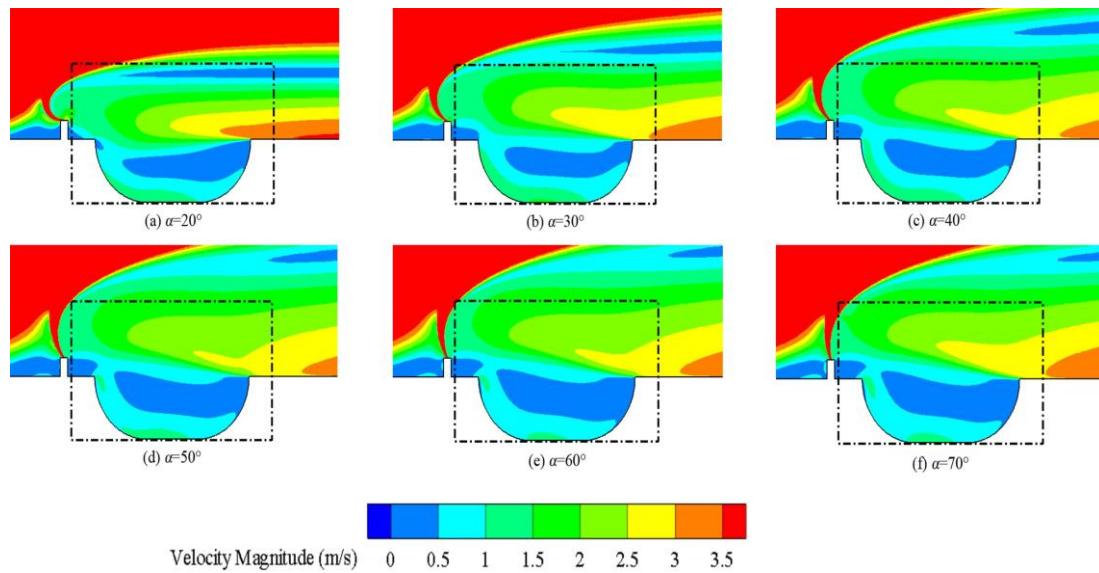


**Fig. 13** Velocity magnitude field at various jet emission angles of the air curtain when  $V$  is 40 m/s ( $\beta$  is 4.0) and  $h$  is 2 m

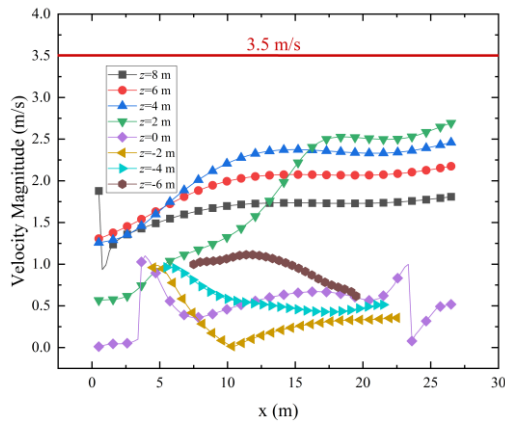


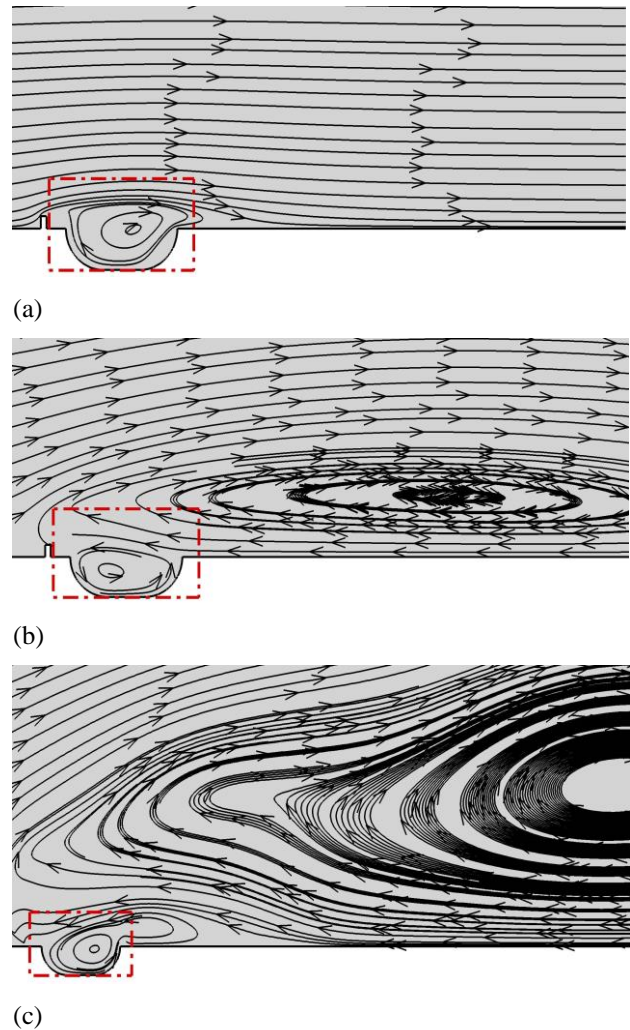
**Fig. 14** Wind velocity magnitude on the segments shown in Figure 11(a) when the jet emission angle  $\alpha$  is  $50^\circ$

### 3.3 Jet in A Crossflow (JICF) Phenomenon in this Study

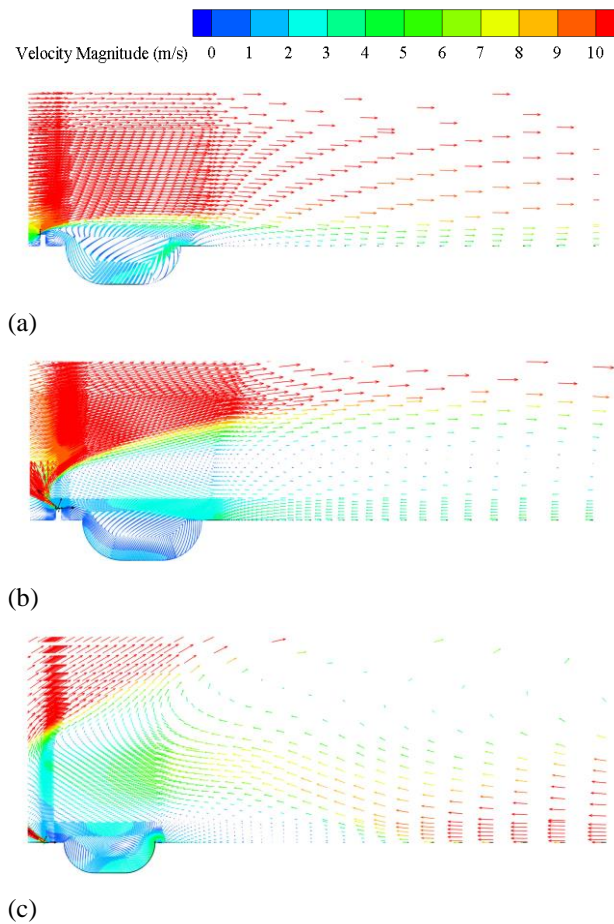
The jet flow produced by the air curtain can generate the JICF phenomenon. To investigate the interaction between the jet flow and the freestream, the streamline diagrams of three cases are displayed in Fig. 15: (a) a 2 m height windbreak without the air curtain, (b) a 2 m height windbreak with the air curtain when  $V$  is 40 m/s ( $\beta$  is 4.0) and  $\alpha$  is  $30^\circ$ , and (c) a 0 m height windbreak with the air curtain when  $V$  is 40 m/s ( $\beta$  is 4.0) and  $\alpha$  is  $30^\circ$ .

Figure 15(a) shows that when the air curtain does not exist, there is only one vortex inside the half-pipe venue. This vortex is due to the combination of the geometric features of this half-pipe venue and the windbreak.

When the air curtain is implemented at the top of the windbreak, as shown in Fig. 15(b), a CRVP obviously forms: one vortex is inside the half-pipe venue, and the other is in the downstream region of the half-pipe venue. This CRVP phenomenon is deemed the most prominent



**Fig. 15** Streamline diagram for (a) a 2 m height windbreak without the air curtain; (b) a 2 m height windbreak with the air curtain when  $V$  is 40 m/s ( $\beta$  is 4.0) and  $\alpha$  is  $30^\circ$ ; (c) a 0 m height windbreak with the air curtain when  $V$  is 40 m/s ( $\beta$  is 4.0) and  $\alpha$  is  $30^\circ$



**Fig. 16 Velocity vector diagram of (a) 2 m height windbreak without air curtain; (b) 2 m height windbreak with air curtain when  $V$  is 40 m/s ( $\beta$  is 4.0) and  $\alpha$  is  $30^\circ$ ; (c) 0 m height windbreak with air curtain when  $V$  is 40 m/s ( $\beta$  is 4.0) and  $\alpha$  is  $30^\circ$**

feature of the JICF when the velocity ratio between the jet flow and the freestream is relatively large (Mahesh, 2013). This feature is usually obtained in experiments (Smith & Mungal, 1998; Recker et al., 2010; Cambonie et al., 2013; Dai et al., 2016; Nair et al., 2019) and 3D numerical simulations (Viti et al., 2009; Rana et al., 2011; Dai et al., 2019; Zhao et al., 2022; Nair et al., 2023), including LES and URANS turbulence models. Herein, the results in Fig. 15(b) indicate that the CRVP can be observed by the 2D URANS model with a velocity ratio of 4.0 and a relatively high Reynolds number of  $4.8 \times 10^6$ . Additionally, the counter direction movement of the air flow between these two vortices causes a low velocity magnitude inside the critical area, which leads to good wind-blocking performance.

When the windbreak is removed and only the air curtain is left to emit the jet flow, the streamline is as shown in Fig. 15(c). One vortex of the CRVP, which rotates in the clockwise direction, becomes extremely large and cannot be fully presented in the figure. Moreover, the negative pressure generated by this vortex results in the other vortex of the CRVP, which is inside the half-pipe venue, moving in the downstream direction.

Moreover, notably, when the air curtain does not exist, the rotation direction of the vortex inside the half-pipe venue is clockwise. However, when the air curtain is on, the rotation direction of this vortex is counterclockwise. Therefore, the jet flow emitted by the air curtain changes the rotation direction of the vortex inside the half-pipe venue.

Figure 16 presents the velocity vector of these three cases. It can be seen that when the jet is emitted without a windbreak (0 m), the velocity near the ground in the downstream region is larger compared to the scenario with a 2 m windbreak. In other words, the 2 m windbreak can block the suction effect near the ground in the downstream region. That could be the reason for the difference between the streamlines shown in Fig. 15 (b) and (c).

#### 4. CONCLUSIONS AND FUTURE WORK

This study investigated the wind-blocking effect of an innovative system composed of a windbreak and an air curtain for half-pipe skiing, which is one of the most popular events at Winter Olympics. This system can both provide an optimal observation viewing experience and satisfy the wind speed standard specified by the FIS in the critical area. To verify and validate the numerical method, a mesh independence study, a time step independence study, and a comparison between the 2D and 3D models were performed first. Then, different heights of the windbreak in this system were numerically investigated, and the impact on the wind-blocking efficiency was studied using both quantitative and qualitative methods. Afterward, the optimal jet emission angle of the air curtain was determined by using a similar strategy as in the windbreak height study. Eventually, the optimal design of this wind-blocking system for this half-pipe skiing sport was established. Additionally, the corresponding aerodynamic phenomena were analyzed and explained. The observations are consistent with previous research mentioned above.

From the current study, the most important discovery is that an air curtain with appropriate jet emission speed (40 m/s) and angle ( $50^\circ$ ) combined with a relatively short windbreak (2 m) can offer a satisfactory wind-blocking effect for the half-pipe skiing sport. This is a significant improvement compared to the vertical dimension of the traditional windbreak used for winter sports (14-15 m). Specifically, the following conclusions are summarized:

- An air curtain can significantly improve the wind-blocking efficiency of this system. Specifically, after adopting an air curtain, the wind-blocking efficiency of a 2 m windbreak can increase from approximately 30% to over 75%, which is more than doubled, on both sides of the half-pipe venue.
- In this system composed of an air curtain and a windbreak, with increasing height of the windbreak, the wind-blocking efficiency will also increase. In particular, the wind-blocking efficiency on the upstream side of the half-pipe venue is consistently higher than that on the downstream side. Considering the purpose of reducing the height of the windbreak, the windbreak height is set to 2 m.

- For fixed windbreak height (2 m) and jet emission speed (40 m/s), the optimal jet emission angle is 50°. This design can guarantee that the wind velocity magnitude inside the critical area is less than the standard set by the FIS.
- This system is actually a JICF. With a relatively high velocity ratio between the jet and freestream, a CRVP appears. This phenomenon was usually obtained in experiments and 3D numerical simulation in previous studies. Thus, the results of the 2D numerical simulations in this study are consistent with those previously obtained by other researchers. Moreover, this CRVP leads to a low velocity magnitude inside the critical area. The JICF will affect the rotation direction of the vortex inside the half-pipe venue.

This study is the first step toward designing an air curtain system with a remarkable wind-blocking effect and a good viewing experience for half-pipe skiing. As observed, the 2D numerical studies can capture the key flow features, such as the CRVP, and reveal that this CRVP leads to a low velocity magnitude inside the critical area. To further investigate the crosswind effects on the athlete, the following issues are recommended to be focused on: (1) a study of the fluctuating wind speed with athlete models, in which a 3D model is necessary and the turbulence effect is considered, and (2) experimental tests of this model in a wind tunnel on a small scale or field tests of a real prototype.

#### ACKNOWLEDGMENTS

This study was funded by the Natural Science Foundation of Hebei Province (A2022210025), which was received by Kan Liu.

#### CONFLICT OF INTEREST

The authors declare that they have no conflicts of interest.

#### AUTHOR CONTRIBUTIONS

**Kan Liu:** Conceived and designed the study; wrote the manuscript; reviewed and edited the manuscript; **Fangyuan Liu:** Conducted the experiments/data collection; analyzed the data; **Qingkuan Liu:** Provided overall supervision for the project; provided critical insights and feedback during the study design and manuscript preparation.

#### DATA AVAILABILITY STATEMENT

The data that support the findings of this study are available on request from the corresponding author, Q. Liu. The data are not publicly available because they contain information that could compromise the privacy of research participants.

#### REFERENCES

- Bidan, G., & Nikitopoulos, D. E. (2013). On steady and pulsed low-blowing-ratio transverse jets. *Journal of Fluid Mechanics*, 714, 393–433. <https://doi.org/10.1017/jfm.2012.482>
- Bushnell, H. (2023). *Wind-related injury count reaches double digits at PyeongChang Olympics*. *Yahoo Sport*. (accessed 03-29, 2023)
- Cambonie, T., & Aider, J. L. (2014). Transition scenario of the round jet in crossflow topology at low velocity ratios. *Physics of Fluids*, 26, 084101. <https://doi.org/10.1063/1.4891850>
- Cambonie, T., Gautier, N., & Aider, J. L. (2013). Experimental study of counter-rotating vortex pair trajectories induced by a round jet in cross-flow at low velocity ratios. *Experiments in Fluids*, 54, 1475. <https://doi.org/10.1007/s00348-013-1475-9>
- Cameron, R. W. F., Taylor, J., & Emmett, M. (2015). A Hedera green façade – Energy performance and saving under different maritime-temperate, winter weather conditions. *Building and Environment*, 92, 111–121. <https://doi.org/10.1016/j.buildenv.2015.04.011>
- Chu, C. R., Chang, C. Y., Huang, C. J., Wu, T. R., Wang, C. Y., & Liu, M. Y. (2013). Windbreak protection for road vehicles against crosswind. *Journal of Wind Engineering and Industrial Aerodynamics*, 116, 61–69. <https://doi.org/10.1016/j.jweia.2013.02.001>
- Dai, C., Jia, L., Zhang, J., Shu, Z., & Mi, J. (2016). On the flow structure of an inclined jet in crossflow at low velocity ratios. *International Journal of Heat and Fluid Flow*, 58, 11–18. <https://doi.org/10.1016/j.ijheatfluidflow.2015.12.001>
- Dai, C., Shu, Z., & Mi, J. (2019). Quantitative investigation on the formation of counter-rotating vortex pairs from the inclined jet in crossflow. *Fluid-Structure-Sound Interactions and Control: Proceedings of the 4th Symposium on Fluid-Structure-Sound Interactions and Control*. [https://doi.org/10.1007/978-981-10-7542-1\\_19](https://doi.org/10.1007/978-981-10-7542-1_19)
- Dong, Z., Luo, W., Qian, G., & Wang, H. (2007). A wind tunnel simulation of the mean velocity fields behind upright porous fences. *Agricultural and Forest Meteorology*, 146, 82–93. <https://doi.org/10.1016/j.agrformet.2007.05.009>
- Fang, H., Wu, X., Zou, X., Yang, X. (2018). An integrated simulation-assessment study for optimizing wind barrier design. *Agricultural and Forest Meteorology*, 263, 198–206. <https://doi.org/10.1016/j.agrformet.2018.08.018>
- Fu, Z., & Li, Q. (2023). Study on Wind-Proof Effect and Stability of Windbreak Fence in Alpine Skiing Center. *Sustainability*, 3369. <https://doi.org/10.3390/su15043369>
- Gevorkyan, L., Shoji, T., Peng, W., & Karagozian, A. (2018). Influence of the velocity field on scalar

- transport in gaseous transverse jets. *Journal of Fluid Mechanics*, 834, 173–219. <https://doi.org/10.1017/jfm.2017.621>
- Gillies, J. A., Etyemezian, V., Nikolich, G., Glick, R., Rowland, P., Pesce, T., & Skinner, M. (2017). Effectiveness of an array of porous fences to reduce sand flux: Oceano Dunes, Oceano CA. *Journal of Wind Engineering and Industrial Aerodynamics*, 168, 247–259. <https://doi.org/10.1016/j.jweia.2017.06.015>
- Hamlet, M. P. (1988). Army Research Inst Of Environmental Medicine Natick Ma Natick. Winter sports medicine, (p.0022)
- Heisler, G. M. (1991). Computer simulation for optimizing windbreak placement to save energy for heating and cooling buildings. <https://www.semanticscholar.org/paper/Computer-simulation-for-optimizing-windbreak-to-for-Heisler/ee64d7f83df7d74047bddf6f6f680f4788b25895>
- Jiang, X., Yin, Z., & Cui, H. (2019). Wind tunnel tests of wind-induced snow distribution for cubes with holes. *Advances in Civil Engineering*, 2019, 1–12. <https://doi.org/10.1155/2019/4153481>
- Jones, M., & Yamaleev, N. (2012). *The effect of a gust on the flapping wing performance*. 50th AIAA Aerospace Sciences Meeting Including the New Horizons Forum and Aerospace Exposition. American Institute of Aeronautics and Astronautics, Nashville, Tennessee. <https://doi.org/10.2514/6.2012-1080>
- Klotz, L., Goujon-Durand, S., Rokicki, J., & Wesfreid, J. E. (2014). Experimental investigation of flow behind a cube for moderate Reynolds numbers. *Journal of Fluid Mechanics*, 750, 73–98. <https://doi.org/10.1017/jfm.2014.236>
- Klotz, L., Gumowski, K., & Wesfreid, J. E. (2019). Experiments on a jet in a crossflow in the low-velocity-ratio regime. *Journal of Fluid Mechanics*, 863, 386–406. <https://doi.org/10.1017/jfm.2018.974>
- Li, B., & Sherman, D. J. (2015). Aerodynamics and morphodynamics of sand fences: A review. *Aeolian Research*, 17, 33–48. <https://doi.org/10.1016/j.aeolia.2014.11.005>
- Li, W., Wang, F., & Bell, S. (2007). Simulating the sheltering effects of windbreaks in urban outdoor open space. *Journal of Wind Engineering and Industrial Aerodynamics*, 95, 533–549. <https://doi.org/10.1016/j.jweia.2006.11.001>
- Liu, K., Yu, M., & Zhu, W. (2019). Enhancing wind energy harvesting performance of vertical axis wind turbines with a new hybrid design: A fluid-structure interaction study. *Renewable Energy*, 140, 912–927. <https://doi.org/10.1016/j.renene.2019.03.120>
- Mahesh, K. (2013). The Interaction of jets with crossflow. *Annual Review of Fluid Mechanics*, 45, 379–407. <https://doi.org/10.1146/annurev-fluid-120710-101115>
- Margason, R. J. (1993). *Fifty years of jet in cross flow research*. AGARD.
- Mullin, E. (2023). Aaron Blunck Ends Halfpipe With Frightening Fall, David Wise Races Up Hill to Help. <https://www.nbcsports.com/chicago/beijing-2022-winter-olympics/aaron-blunck-ends-halfpipe-frightening-fall-david-wise-races>
- Nair, V., Krishnan, A., Adhikari, S., Lieuwen, T.C. (2023). *Influence of mixture composition and radial flame location on counter-rotating vortex pair evolution in a reacting jet in crossflow*. AIAA SCITECH 2023 Forum 0344. <https://doi.org/10.2514/6.2023-0344>
- Nair, V., Sirignano, M., Emerson, B., Halls, B., Jiang, N., Felver, J., Roy, S., Gord, J., & Lieuwen, T. (2019). Counter rotating vortex pair structure in a reacting jet in crossflow. *Proceedings of the Combustion Institute*, 37, 1489–1496. <https://doi.org/10.1016/j.proci.2018.06.059>
- Nanda, S. (2012). Preventing cold injuries: Winter safety tips. *Consultant* 360, 11(12).
- New, T. H., Lim, T. T., & Luo, S. C. (2006). Effects of jet velocity profiles on a round jet in cross-flow. *Experiments in Fluids*, 40, 859–875. <https://doi.org/10.1007/s00348-006-0124-y>
- Park, C. W., & Lee, S. J. (2003). Experimental study on surface pressure and flow structure around a triangular prism located behind a porous fence. *Journal of Wind Engineering and Industrial Aerodynamics*, 91, 165–184. [https://doi.org/10.1016/S0167-6105\(02\)00343-4](https://doi.org/10.1016/S0167-6105(02)00343-4)
- Perrotta, G., & Jones, A. R. (2017). Unsteady forcing on a flat-plate wing in large transverse gusts. *Experiments in Fluids*, 58, 101. <https://doi.org/10.1007/s00348-017-2385-z>
- Poudel, N., Yu, M., & Hrynyuk, T. (2021). Gust mitigation with an oscillating airfoil at low Reynolds number. *Physics of Fluids*, 33, 101905. <https://doi.org/10.1063/5.0065234>
- Rana, Z. A., Thornber, B., & Drikakis, D. (2011). Transverse jet injection into a supersonic turbulent cross-flow. *Physics of Fluids*, 23, 046103. <https://doi.org/10.1063/1.3570692>
- Recker, E., Bosschaerts, W., Wagemakers, R., Hendrick, P., Funke, H., & Börner, S. (2010). *Experimental study of a round jet in cross-flow at low momentum ratio*. 15th International Symposium on Applications of Laser Techniques to Fluid Mechanics Lisbon 05–08.
- Regan, M. A., & Mahesh, K. (2017). Global linear stability analysis of jets in cross-flow. *Fluid Mech*, 828, 812–836. <https://doi.org/10.1017/jfm.2017.489>
- Sau, R., & Mahesh, K. (2008). Dynamics and mixing of vortex rings in crossflow. *Journal of Fluid*

- Mechanics*, 604, 389–409.  
<https://doi.org/10.1017/S0022112008001328>
- Smith, S. H., & Mungal, M. G. (1998). Mixing, structure and scaling of the jet in crossflow. *Journal of Fluid Mechanics*, 357, 83–122.  
<https://doi.org/10.1017/S0022112097007891>
- Suresh, S. (2006). Winter sports injuries: patterns of injury--preventive measures. *Contemporary Pediatrics*, 5(3).
- Tominaga, Y., & Shirzadi, M. (2022). RANS CFD modeling of the flow around a thin windbreak fence with various porosities: Validation using wind tunnel measurements *Journal of Wind Engineering and Industrial Aerodynamics*, 230, 105176  
<https://doi.org/10.1016/j.jweia.2022.105176>
- TRTWorld (2023). Injuries and chaos as icy winds disrupt events at Pyeongchang Games. <https://www.trtworld.com/sport/injuries-and-chaos-as-icy-winds-disrupt-events-at-pyeongchang-games-15100>(accessed 03-29, 2023)
- Viti, V., Neel, R., & Schetz, J. A. (2009). Detailed flow physics of the supersonic jet interaction flow field. *Physics of Fluids*, 21, 046101.  
<https://doi.org/10.1063/1.3112736>
- Zhang, X., Tse, K. T., Weerasuriya, A. U., Li, S. W., Kwok, K. C. S., Mak, C. M., Niu, J., & Lin, Z. (2017). Evaluation of pedestrian wind comfort near ‘lift-up’ buildings with different aspect ratios and central core modifications. *Building and Environment*, 124, 245–257. <https://doi.org/10.1016/j.buildenv.2017.08.012>
- Zhao, Z., Wang, S., Tang, X., Song, J., & Wang, Z. (2022). Large eddy simulation of compound angle film cooling with vortex generators. *International Journal of Thermal Sciences*, 178, 107611.  
<https://doi.org/10.1016/j.ijthermalsci.2022.107611>
- Zhu, S., Gao, N., & Ye, Y. (2022). Numerical simulation to assess the impact of urban green infrastructure on building energy use: A review. *Building and Environment*, 109832  
<https://doi.org/10.1016/j.buildenv.2022.109832>